

Automated preclinical detection of mechanical pain hypersensitivity and analgesia

Zihe Zhang^{a,b}, David P. Roberson^{a,b}, Masakazu Kotoda^{a,b}, Bruno Boivin^{a,b}, James P. Bohnslav^b, Rafael González-Cano^{a,b}, David A. Yarmolinsky^{a,b}, Bruna Lenfers Turnes^{a,b}, Nivanthika K. Wimalasena^{a,b}, Shay Q. Neufeld^b, Lee B. Barrett^{a,b}, Nara L. M. Quintão^{a,b}, Victor Fattori^{a,b}, Daniel G. Taub^{a,b}, Alexander B. Wiltschko^b, Nick A. Andrews^{a,b}, Christopher D. Harvey^b, Sandeep Robert Datta^b, Clifford J. Woolf^{a,b,*}

Abstract

The lack of sensitive and robust behavioral assessments of pain in preclinical models has been a major limitation for both pain research and the development of novel analgesics. Here, we demonstrate a novel data acquisition and analysis platform that provides automated, quantitative, and objective measures of naturalistic rodent behavior in an observer-independent and unbiased fashion. The technology records freely behaving mice, in the dark, over extended periods for continuous acquisition of 2 parallel video data streams: (1) near-infrared frustrated total internal reflection for detecting the degree, force, and timing of surface contact and (2) simultaneous ongoing video graphing of whole-body pose. Using machine vision and machine learning, we automatically extract and quantify behavioral features from these data to reveal moment-by-moment changes that capture the internal pain state of rodents in multiple pain models. We show that these voluntary pain-related behaviors are reversible by analgesics and that analgesia can be automatically and objectively differentiated from sedation. Finally, we used this approach to generate a paw luminance ratio measure that is sensitive in capturing dynamic mechanical hypersensitivity over a period and scalable for high-throughput preclinical analgesic efficacy assessment.

Keywords: Preclinical pain models, Machine learning, Machine vision, Automated pain detection

1. Introduction

Current behavioral assessments of pain in preclinical models^{11,26} are essentially based on 3 distinct approaches: (1) reflex

Sponsorships or competing interests that may be relevant to content are disclosed at the end of this article.

Z. Zhang and D. P. Roberson contributed equally to this manuscript.

^a Boston Children's Hospital, F.M. Kirby Neurobiology Center, Boston, MA, United States. D.P. Roberson is now with Blackbox Bio, LLC, Dallas, TX, United States. R. González-Cano is now with the Department of Pharmacology, University of Granada, Granada, Spain. N.K. Wimalasena is now with Decibel Therapeutics, Boston, MA, United States. N.L.M. Quintão is now with the Postgraduate Programme in Pharmaceutical Science, Universidade do Vale do Itajaí (UNIVALI), Itajaí, Santa Catarina, Brazil. V. Fattori is now with the Laboratory of Pain, Inflammation, Neuropathy, and Cancer, Department of Pathology, Londrina State University, Londrina, Paraná, Brazil. A.B. Wiltschko is now with the Google Research, Brain Team, Cambridge, MA, United States. N.A. Andrews is now with the Salk Institute for Biological Studies, La Jolla, CA, United States, ^b Department of Neurobiology, Harvard Medical School, Boston, MA, United States

*Corresponding author. Address: Boston Children's Hospital, 300 Longwood Avenue, CLS 12258, Boston, MA, United States. E-mail address: clifford.woolf@childrens.harvard.edu (C. J. Woolf).

Supplemental digital content is available for this article. Direct URL citations appear in the printed text and are provided in the HTML and PDF versions of this article on the journal's Web site (www.painjournalonline.com).

PAIN 163 (2022) 2326–2336

Copyright © 2022 The Author(s). Published by Wolters Kluwer Health, Inc. on behalf of the International Association for the Study of Pain. This is an open access article distributed under the terms of the Creative Commons Attribution-Non Commercial-No Derivatives License 4.0 (CCBY-NC-ND), where it is permissible to download and share the work provided it is properly cited. The work cannot be changed in any way or used commercially without permission from the journal.

<http://dx.doi.org/10.1097/j.pain.0000000000002680>

withdrawal-based assays of sensitivity to acute mechanical and thermal stimuli, (2) operant conditioning-based assays targeting the aversive nature of pain and the rewarding nature of pain relief,³⁰ and (3) quantification of behavioral features altered or induced by pain, which includes 2 general categories: first, detection of behaviors such as the frequency of biting and/or licking of a paw in pain,¹ home-cage behavior,³⁷ or facial grimaces¹⁶ and second, changes in dynamic/static weight-bearing^{14,31} and locomotor gait.³⁶

Pain assays based on the first and second approaches have several major limitations. The von Frey test that quantifies the force required to prompt paw withdrawal after a static punctate mechanical stimulus to the skin, eg, has been widely used both for laboratory pain research and analgesic efficacy determination. Although high-speed videography and machine learning can make the von Frey test more objective and sensitive,^{2,13} the von Frey test and other related stimulus-evoked tests only capture snapshots of pain dynamics, conflate sedation and analgesia, and require extensive animal-human observer interaction, which modifies animal behavior and introduces variability to the behavioral readout.²⁸ On the other hand, conditioning-based assays are not practical for large-scale analgesic efficacy validation because they are time-consuming and influenced by nonanalgesic drug effects, particularly those associated with abuse liability.

Pain assays that can detect changes in the behavior of a freely moving animal for long periods will circumvent many of these limitations and can be automated with use of machine vision and learning. Human-defined behaviors, such as facial grimacing and paw biting/licking, have been used to indicate pain and assess analgesic actions in rodents,^{1,16} and deep learning improves and

automates the scoring of these user-defined pain-related behaviors.^{6,16,29} On the other hand, movement analyses originally developed for studying the neural circuits underlying locomotor function in rodents^{4,18,33} have been applied to assaying single hind limb-based pain models^{4,36} and reveal that limb pain induces changes in locomotion. We believe that the combination of both a bottom-up view angle of body pose to detect body position and movement and a luminance-based paw surface contact measurement (using frustrated total internal reflection technology,³³ FTIR) may be advantageous in capturing exactly how unilateral limb pain affects the avoidance of surface contact and drives or changes distinct behaviors, such as standing, rearing, scratching, paw biting, or grooming, as well as locomotion, over long periods, in freely behaving animals in the absence of an observer.

2. Methods

2.1. Experimental subjects

Adult (10-15-week-old) male and female C57BL6/J mice (Jackson Laboratory, Bar Harbor, ME) were housed in standard clear plastic cages with no more than 5 animals per cage under controlled conditions (lights on 07:00-19:00; humidity 30%-50%; temperature 22-23°C) with ad libitum access to food and water. All experiments were performed between 9:00 and 17:00 in a room maintained at a temperature of $21 \pm 1^\circ\text{C}$. All experimental protocols comply with relevant ethical regulations and were approved by Boston Children's Hospital Institutional Animal Care and Use Committee. Animals were randomized to treatment groups.

2.2. Design of the bottom-up paw luminescence and pose capture apparatus

The animal containment chamber consisted of an 18 (l) \times 18 (w) \times 15-cm (h) black acrylic box that was closed on all sides except for the bottom. It was placed on a 25-cm square piece of 5-mm thick borosilicate float glass, the "floor". Eight hundred fifty nanometers near-infrared (NIR) LED strips (SMD3528-600-IR, Huake Light Electronics Co, Ltd, Shenzhen, China) were aligned perpendicular to 2 opposing edges of the glass and held in place using t-slot aluminum extrusions. Beneath the floor, a camera enclosure was built using opaque black acrylic panels to prevent light from entering the black box from below. A 25 \times 25-cm black acrylic surround panel with an 18 \times 18-cm square cutout was positioned on top of the glass floor panel to prevent light from entering the camera enclosure from above. Two separate 850-nm NIR LED strips (SMD5050-300-IR, Huake Light Electronics Co, Ltd, Shenzhen, China) were positioned horizontally 10 cm below the glass floor to provide illumination of the animals from below and positioned such that reflections from the LEDs off of the sides, top, or floor of the chamber are not visible from the camera position.²⁵ Power to all LEDs was provided by a 12-V DC power supply.

2.3. Recording setup

An NIR camera (Basler acA2000-50gmNIR GigE) located 30 cm beneath the glass surface was used to record animals in the dark. The Pylon viewer software (v4.1.0.3660) provided by the camera manufacturer was used to initiate video recordings. Camera settings were stored and loaded from a pylon feature stream file (*.pfs) to ensure the same parameters were used for each recording. Frames were acquired at 50 Hz with dimensions 1000

\times 1000 pixels. Unless noted otherwise, all frames were downsized for analysis to 500 \times 500 pixels using ImageJ's scaling function, specifying to average when downsizing. A Raspberry Pi microcomputer was used to switch power on and off to the LED strips below the glass floor on alternating video frames based on a frame initiation signal generated by the camera.

2.4. Hardware for data analysis

Machine learning analyses were performed using a consumer-grade PC with an Intel i7-8700K CPU, 64 GB RAM, and NVIDIA 1080Ti GPU.

2.5. Determination of general activity levels

Animals were placed in individual chambers within the device and recorded for 1 hour at 30 frames per second (fps).³² Python (v3.7.3) script was designed to process the recordings using the Computer Vision Library OpenCV (v4.1.0). Videos were down-sampled temporally by a factor of 3, and individual chambers spatially separated for parallel processing of animals. For each recording and each grayscale frame, a binary threshold was used to set pixels with values greater than 2.3 times the frame mean, ie, 255, a threshold we heuristically found to help our measurements reflect movement and exclude noise. Background subtraction was achieved using the Gaussian mixture-based background/foreground segmentation algorithm using OpenCV's *createBackgroundSubtractorMOG2* function, setting the history parameter to 100, determined to be optimal after varying its value and empirically evaluating performance. Temporal variations in the average of the differential binary mask, reflective of the proportion of the mouse pixels that moved, were used as a measure of activity over time, with the caveat that behaviors such as rearing, where upper-body movement is occluded by the posture of the animal and not fully detectable from this measurement, may result in low movement values. Values lower than 5, between 5 and 20, and higher than 20 were labeled as no activity, low activity, and high activity, respectively. These unitless demarcations, reflective of pixel changes, were set heuristically to separate displacement of the entire body (values beyond 20) from small in-place movements such as slight head rotation or paw shifts (values between 5 and 20). The bottom delimitation (values less than 5) helped capture and exclude noise and movements due to breathing. Summation of the number of frames in each activity level allowed comparison of the time spent in each category.

2.6. Tracking of individual body parts

Five naive mice and 5 formalin-stimulated mice were each recorded for 1 hour at 50 Hz. For each mouse, 50 body frames (500 \times 500 pixels) were randomly selected and the center point of each of the 4 paws, the snout, the centroid, and the tail base were manually labeled using DeepLabCut software. The 500 frames and the corresponding 3500 labeled data points were used to train the open-source neural network DeepLabCut (v1.0). The DeepLabCut model achieved a training error of 1.32 pixels and a test error of 1.64 pixels across all body parts. The tracking for centroid had a training error of 1.28 pixels and a test error of 1.39 pixels. The model was specifically trained against video frames containing feces in the field of view to overcome potential interference. The trained model was used to automatically determine the location of all 7 points of interest on new videos.

2.7. Paw luminance measurements

For a given recording, for each pair of body frame and FTIR frame, the locations of each hind paw were identified using the body frame, using the DeepLabCut neural network. Individual paw recordings were generated by extracting an area of size 23×23 squared pixels centered at the predicted paw location on each FTIR frame, and paw luminance measured as the average brightness of the FTIR signal in the area.

2.8. Force-to-luminance scale

A 3D-printed plastic disk attached to a force transducer was used to collect force measurements through a MATLAB interface while simultaneously recording hind paw luminance using our apparatus. The experiment was performed with a single anesthetized C57BL/6J mouse with its hind limb taped in-place to the glass surface.

2.9. Automated classification of face and body grooming behaviors

Scoring of face and body grooming is important in a range of neurobehavioral assays including those related to pain and itch,^{3,24,27} which has been notoriously difficult because limb movements remain close to the body and cannot be readily differentiated with a top-down viewpoint. Twenty-eight ($n = 28$) wild-type C57BL/6J mice were recorded in the apparatus collecting 419,846 frames, each manually labeled using a custom MATLAB interface for 1 of 3 behaviors: face grooming (5% of all frames), body grooming (24%), or other (71%). Videos were reconstructed by stacking corresponding body-FTIR pairs with their mean, yielding 3-channel videos like the standard 3-channel RGB format. All videos were downsized in dimensions to 250×250 pixels using the approach described above and placed in 1 of 3 data sets: training (22 videos), validation (3), and test (3). All videos were spatially aligned and cropped using our centering and alignment procedure.

Frames were first aligned spatially along the vector connecting the tail base to the centroid of the animal. Specifically, frames were rotated to align the animal orientation with the positive y-axis of the Cartesian plane (pointing upward). Background pixels, identified as those pixels outside the binary body mask generated while computing the centroid, were set to 0. The aligned frames are the input for automatic behavior scoring.

The convolutional neural network, described in Supplementary Figure S2C (available at <http://links.lww.com/PAIN/B641>), was implemented using PyTorch (v1.4), taking input video frames and generating vectors of 3 probabilities, 1 for each behavior of interest. Probability thresholds were set to maximize the F1 score on the validation data set. Similarly, all hyperparameters were optimized using random searches and set to maximize the F1 score on the validation set. Frames in which both face and body grooming predictions were below threshold were automatically set to other behaviors.

The model used a multiclass cross-entropy loss function weighted by the fraction of observed positives, further penalizing the model for errors on rare behaviors. We used the Adam (Adaptive Moment Estimation) optimizer¹⁵ with an initial learning rate of 10^{-4} set to decay at a rate of 10 on saturation of performance on the validation set for more than 10,000 training steps, which we heuristically found to help improve performance. The model was trained over 55,000 training steps. Each training step consists of a forward pass of the network on 1 batch of data, followed by a backward pass and 1 optimizer step in the downward direction of the gradients.

The perbehavior F1 scores were calculated with respect to the manual labels and shuffled labels, where we randomly shuffled manual labels 100 times and calculated the F1 score for each shuffle. F1 scores on the test set (background: 0.96059 (true labels), 0.678 ± 0.067 (shuffled labels, mean \pm SD); face grooming: 0.39902, 0.078 ± 0.030 ; body grooming: 0.90059, 0.341 ± 0.127) demonstrate a decent classification performance for both face and body grooming. Further improvements on the classification performance could be made by adopting more sophisticated neural network structures.

2.10. Automated scoring of paw-biting behavior

We designed and trained a convolutional neural network with a similar architecture as that described above for classifying single frames of videos into “paw biting” or “not paw biting”. The classifier was trained on 8 videos of formalin-stimulated mice. The probability threshold was set as 0.5 for classifying new frames. The scoring of paw biting is defined as the time an animal spent biting its injured paw in each 5-minute bins after formalin injection. When scoring an unseen video, the automatic scorer first classifies each single frame, then calculates the percentage of frames classified as paw biting in each 5-minute bins and converts it to the time spend as paw biting. We tested the scorer on 8 videos of formalin-stimulated mice and compared its performance to human labeling. In 4 of those 8 videos, mice were treated with morphine before the formalin test.

2.11. Paw luminance measurements as an indicator of pain behavior and analgesia

To pool the paw luminance measures of individual animals, the paw luminance values for each animal were first scaled with a min-95 quantile scaler such that all data points for a single recording were first subtracted by the minimum value and then divided by the difference between the 95th quantile and the minimum value.

2.12. Tracking locomotion

For a given recording, the location of tail base was extracted from body frames using the DeepLabCut. The distance traveled from frame to frame was calculated as the Euclidean distance between the locations of tail base in consecutive body frames. The accumulative locomotion over time, in the unit of pixel distance, was defined as the sum of the distance traveled from frame to frame.

2.13. von Frey test

Mice were habituated to the testing environment over 3 independent sessions of 1 hour each conducted on consecutive days. Mechanical hypersensitivity was assessed using von Frey filaments applied to the affected hind paw, with a positive response consisting of a paw lifting or flinching response to the fiber. The response patterns were collected and converted into corresponding 50% withdrawal thresholds using the Up-Down Reader¹⁰ software and associated protocol. Treatments were randomized, and all tests were performed by investigators blinded to the treatments.

2.14. Intraplantar formalin injection

C57BL6/J male mice were given an intraplantar injection of formalin (5%, 10 μ L/paw) in the left hind paw and subsequently recorded in the enclosure.

2.15. Morphine treatment

Mice were injected subcutaneously with morphine (3 mg/kg morphine dissolved in 0.3 mg/mL saline solution; NDC 0641-6127-25, WEST-WARD, Eatontown, New Jersey) or saline control 30 minutes before formalin injection.

2.16. Paw-biting behavior

Sixteen adult (8-10-week-old) C57BL6/J male mice were given intraplantar formalin treatment and recorded for 40 minutes. Four of the 16 mice were treated with subcutaneous morphine injection. All videos were manually scored for paw-biting behavior, and the scorings were used for training of the paw-biting algorithms.

2.17. Ultraviolet radiation burn model

Six C57BL6/J male mice were anesthetized with 3% isoflurane. UV irradiation was performed on the left hind paw under sustained anesthesia with 1.5% isoflurane at an intensity of 1 J/cm² for 2 minutes using a wavelength of 305 to 315 nm using a fluorescent UV-B light source (XR UV LEDs 308 nm, RayVio, Hayward, California). Forty-eight hours after irradiation, the von Frey test was performed, and the mice were recorded for 10 minutes in the enclosure. Another set of 5 mice received only isoflurane anesthesia without UV irradiation and used as a control.

2.18. Zymosan inflammation model

Inflammatory pain was induced by zymosan injection in 5 female C57BL6/J mice. The left hind paw was injected subcutaneously with 20 μ L of zymosan (5 mg/mL in saline; Z4250, Sigma-Aldrich, St. Louis, Missouri). Four hours after the injection, the von Frey test was performed, and the mice were recorded for 10 minutes in our enclosure. Another set of 5 mice were injected with only saline and used as a control.

2.19. Paw skin incision model

Eight male mice were anesthetized with 2% isoflurane, and a 5-mm longitudinal skin incision was made on the plantar surface of the left hind paw using a number 11 surgical blade. The incision was superficial, and the subdermal tissue was not exposed or damaged. Mice were returned to their home cage for full recovery from anesthesia before behavioral tests.

2.20. Knee complete Freund adjuvant injection model

Six male mice were anesthetized with 2% isoflurane, and 10 μ L of complete Freund adjuvant (CFA) was injected to the left knee joint using a 31-gauge insulin needle. Mice were recorded 3 days after the CFA injection.

2.21. Spared nerve injury model

Spared nerve injury surgery was performed under isoflurane anesthesia (3% induction/2% maintenance) on adult mice. The skin on the lateral surface of the thigh was incised and a section made directly through the biceps femoris muscle exposing the sciatic nerve and its 3 terminal branches. The tibial and common peroneal branches were tightly ligated with a 5-0 silk suture and transected distally to the ligation, removing 4 \pm 2 mm of the distal

nerve stump, whereas the sural nerve was left intact. After injury, incision was sutured with a 6-0 silk suture, and mice were allowed to recover on heated pads before being returned to their home cage.

2.22. Sciatic nerve crush injury model

Sciatic nerve crush surgery was performed under isoflurane anesthesia (3% induction/2% maintenance) on adult mice. The skin on the lateral surface of the thigh was incised and a section made directly through the biceps femoris muscle exposing the sciatic nerve and its 3 terminal branches. The sciatic nerve was crushed for 10 seconds by a pair of hemostatic forceps. At the end of this procedure, the nerves were completely flattened and transparent. After injury, incision was sutured with a 6-0 silk suture, and mice were allowed to recover on heated pads before being returned to their home cage.

2.23. Sham control for both spared nerve injury and sciatic nerve crush injury models

Sham surgery was performed under isoflurane anesthesia (3% induction/2% maintenance) on adult mice. The skin on the lateral surface of the thigh was incised and a section made directly through the biceps femoris muscle exposing the sciatic nerve and its 3 terminal branches. Then, the incision was sutured with a 6-0 silk suture, and mice were allowed to recover on heated pads before being returned to their home cage.

2.24. Ketorolac treatment in ultraviolet radiation burn model

Ten male C57BL6/J mice received the ultraviolet stimulus described above. Forty-eight hours after UV irradiation, 5 mice were injected intraperitoneally with 10 mg/kg ketorolac dissolved in 250 μ L of saline, whereas the other 5 mice received only saline. One hour after injection, mice were recorded for 10 minutes in our apparatus.

2.25. Ketorolac treatment in zymosan model

A total of 40 male mice were randomly assigned to either the von Frey group or recording group. After baseline session(s), all mice received 20 μ L of zymosan in the left hind paw. Four hours after zymosan injection, another session of either von Frey test or recording in our enclosure was conducted (pretreatment). The mice then received single bolus intraperitoneal injection of ketorolac at doses of 1, 3, or 10 mg/kg, or saline (n = 5 each). One hour later, either von Frey test or recording in the bottom-up device was conducted (posttreatment).

2.26. Diazepam treatment in zymosan model

After baseline session, 5 mice received 20 μ L of zymosan in the left hind paw. Four hours after zymosan injection, another session of recording in our enclosure was conducted (pretreatment). The mice then received single bolus intraperitoneal injection of diazepam at dose of 5 mg/kg. Thirty minutes later, recording in the bottom-up device was conducted (posttreatment).

2.27. Quantification and statistical analysis

Statistical analyses were performed using GraphPad Prism (v. 8.0.0). Data are expressed as mean \pm SEM for mouse

mechanical withdrawal (von Frey) experiments and for comparison of paw luminance values. Tests used for statistical significance are reported in figure legends. *P* values are indicated in figures, with values less than 0.05 considered significant. The number of animals used is defined in figure legends.

3. Results

3.1. Behavioral assessment system for rodent limb pain

We hypothesized that if a disease condition produces mechanical pain hypersensitivity, the force applied to a surface through the painful part of the body will be reduced because of the reduction or avoidance of contact. We sought to test whether a detailed and continuous measurement of the pressure applied to a surface through an affected limb, together with the contextual information of different naturalistic behaviors, would generate a sensitive and dynamic measurement of mechanical pain hypersensitivity, and its disruption by analgesics, in rodent hind limb pain models.

We engineered a device that simultaneously records the pose of a freely moving rodent's body (for applying ethological behavioral analyses) and an FTIR luminance-based signal of paw surface contact as a measure of mechanical sensitivity (**Fig. 1A**, Supplemental Video 1, available at <http://links.lww.com/PAIN/B642> and the Methods section). Body pose is recorded by a camera under a glass surface using NIR transillumination LEDs, which reveal the entire ventral view of the rodent body. Light from a separate set of NIR (850 nm) LEDs enters perpendicular to the edge of the glass sheet to produce an evanescent light field at the planar air–glass interface that is scattered on paw contact to provide a force-sensitive light/luminance signal. This FTIR signal is captured separately from the body pose images by supplying power to the transillumination LEDs only on alternating video frames, revealing footprint contact features of the animal. The FTIR luminance signal is then combined with the body pose recording such that the interleaved imaging channels produce paired video streams of the ventral body pose and the body surface contact, each at 25 fps. The animal is allowed to freely explore in a dark and isolated chamber, which mitigates the potential olfactory, auditory, or visual cues of predators, including investigators in a laboratory setting^{7,28} (Supplemental Fig. S1, available at <http://links.lww.com/PAIN/B641>).

Superimposition of the FTIR signal on body pose recordings reveals rich locomotor information not discernible with either video image alone, such as whether a paw is in contact with the surface or just held close to it, and changes in the shape and area of plantar surface contact of each paw during different behaviors (**Fig. 1B**, Supplemental Video 2, available at <http://links.lww.com/PAIN/B643>). Furthermore, by manually applying force to the paw of an anesthetized mouse using a force transducer while recording the luminance of the paw contact area, we found that FTIR paw luminance increases linearly to the downward force transmitted through the paw to the glass over a physiologically relevant range (0–30 g) (**Fig. 1C**) and is therefore a measure of mechanical contact force. This range is below the saturation level of the FTIR signal and is linear (**Fig. 1C**).

An automatic processing pipeline was constructed for extracting the FTIR luminance signal of both hind paws from the recordings of freely behaving animals (Supplemental Video 3, available at <http://links.lww.com/PAIN/B644>). First, a deep neural network, DeepLabCut,¹⁹ was used on the body pose signal for the tracking of 7 individual body parts (snout, tail base, centroid, and 4 paws). The paw luminance value for each paw at every time point was then determined by first identifying the location of the

paw using the body pose frame and then extracting the average pixel intensity in a square box centered around the paw location in the paired FTIR frame. With this pipeline, dynamic paw luminance signals for each hind paw can be measured as the animal performs naturalistic behaviors, such as walking, where there is a patterned alternating surface contact of each paw (**Fig. 1D**), and the relationship of paw contact to a particular behavior can then be readily assessed. After urination, any wet paw appears brighter in the paw luminance signal. We found that habituation significantly decreased the amount of urine and feces produced during an actual recording period. Therefore, the animals were habituated in the recording device for 30 minutes before video acquisition, and the floor was cleaned before the video acquisition.

3.2. Pain and analgesia signals of acutely induced pain

We first examined whether the FTIR luminance value of each hind paw captures and quantifies key behavioral features of the pain that is induced by the intraplantar injection of formalin and of the analgesia produced by morphine in this model. Plantar formalin injection is an acute nociceptive pain model commonly used in analgesic drug discovery.¹ The formalin injection evokes sustained pain-related behaviors over 30 minutes through activation of nociceptor TRPA1 channels.²⁰ The biphasic paw-biting behavior elicited is a primary pain behavioral readout currently used in preclinical analgesic development and is typically scored manually.

From individual recordings, changes in the behavior of mice on intraplantar injection of formalin in 1 hind paw were combined with an inspection of paw luminance signals (**Fig. 2A**). Although an intraplantar saline injection is considered to represent a “vehicle control”, the paw luminance signals of individual mice from the intraplantar saline injection sham group captured an asymmetry between 2 hind paws, with a lower luminance value of the injected paw, which reflects unilateral increased mechanical pain sensitivity while the mouse was walking and rearing. Paw luminance signals of mice from the intraplantar formalin injection group showed an even greater asymmetry between the 2 hind paws, one that was moreover persistent through all behaviors, reflecting a prominent mechanical pain hypersensitivity induced by formalin injection such that contact of the injected paw with the surface was substantially reduced. Mechanical hypersensitivity in the first 30 minutes immediately after formalin injection, which precedes tissue inflammation, has not been reported before. The analgesia group (subcutaneous morphine (3 mg/kg) and intraplantar formalin injections) showed a restoration of symmetry between 2 hind paws, but this was present only when the mouse was walking, not when rearing or pausing, something that could not be detected without the combined body pose and surface contact measurements. The example traces in **Figure 2A** indicate that the paw luminance ratio can capture the presence of mechanical pain hypersensitivity and its reversal with morphine in the formalin model, as well as novel features of pain-related behavior and analgesia, ie, its onset, duration, and association with locomotory activities of the mouse. Although in the current study we focused on characterizing the changes captured by the average luminance signal, the resolution of the paw luminance signal indicates that subtle differences between animals doing the same behaviors (eg, walking or rearing) in different pain states could be comprehensively characterized with the device.

The temporal dynamics of the paw luminance ratio in the formalin group (*n* = 6) showed a biphasic decrease, with the first phase at 0 to 5 minutes and the second phase at 15 to 30 minutes after formalin injection, capturing the well-described 2 phases of

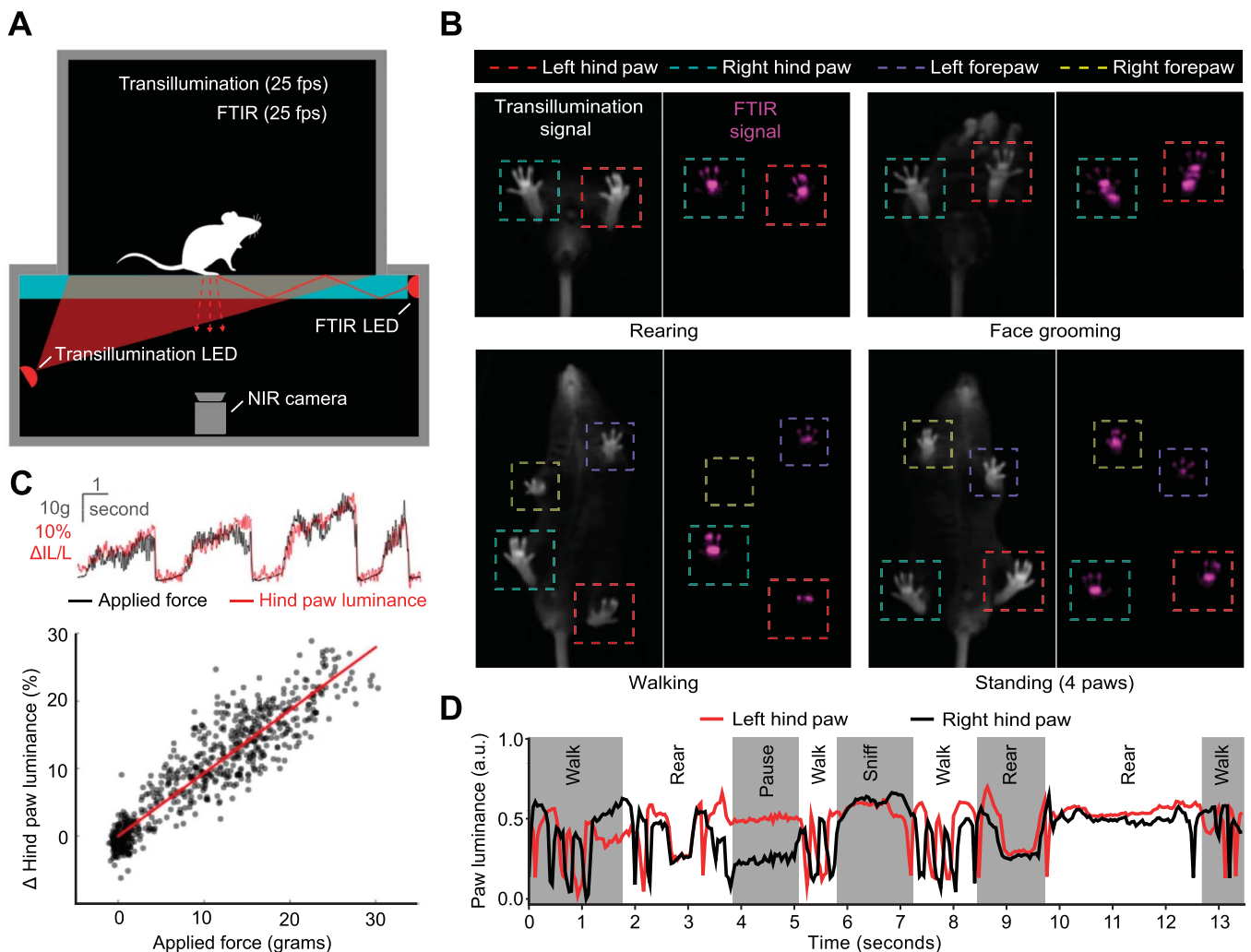


Figure 1. Bottom-up freely moving behavioral assessment system. (A) Schematic of recording device illustrating NIR transillumination and FTIR, captured using a single NIR camera, each at 25 fps. (B) Representative frames from transilluminated (body frame) and FTIR channels. FTIR signal captures subtle footprint patterns of freely moving mice. (C) Relationship between normalized hind paw FTIR luminance signal (red) and force applied to a paw (black). Scatterplot demonstrates linear relationship ($R^2 = 0.85$) between force and luminance over a physiologically relevant range, and data points represent individual force transducer application in a single mouse. (D) Demonstration of dynamic FTIR luminance signals (25 fps) for each hind paw during different naturalistic behaviors. Paw luminance signals are scaled (min-95 quantile) and are shown in arbitrary unit (a.u.). fps, frames per second; FTIR, frustrated total internal reflection; NIR, near-infrared.

pain in the formalin model,¹ whereas the temporal dynamics of the analgesia group ($n = 5$) showed a partial reversal of the first phase and a complete reversal of the second phase towards the baseline levels present in the sham group ($n = 6$) (Fig. 2B). Unilateral formalin injection drove the dynamics of the paw luminance ratio away from the baseline (indicating an asymmetry between ipsilateral (injected) and contralateral (noninjected) hind paws), and its relief by morphine reversed the ratio towards the baseline (Fig. 2C). The change in the paw luminance ratio further indicated a weight redistribution between the ipsilateral and the contralateral hind paws (Supplemental Fig. S2A, available at <http://links.lww.com/PAIN/B641>). We chose a ratio of paw luminance as the readout because it was robust across multiple recordings. The paw luminance ratio is invariant to size differences between animals and to potential calibration differences between recordings by different cameras. The average paw luminance ratio over 30 minutes distinguished the formalin group from the sham and the analgesia groups with P values of 0.0006 and 0.0001, respectively (Fig. 2D), and represents, therefore, a robust measurement of mechanical pain dynamically assessed over time.

In addition to paw luminance measurements, we simultaneously extracted behavioral features from the same set of recordings. This analysis, eg, identified morphine-induced hyperlocomotion, which is a documented side effect of systemic injection of morphine in mice at 3 mg/kg²² (Supplemental Fig. S2B, available at <http://links.lww.com/PAIN/B641>). Based on the body pose recordings, we were also able to implement a supervised deep-learning pipeline that automatically labeled multiple classes of user-defined behaviors, such as face grooming, body grooming, and paw biting (Supplemental Fig. S2C, available at <http://links.lww.com/PAIN/B641>; the Methods section). Using an independently trained automatic paw-biting scorer, we identified the biphasic paw-biting behavior in the formalin model and found a reduction of paw biting in the morphine-treated group (Supplemental Fig. S2D, available at <http://links.lww.com/PAIN/B641>). The combination of paw luminance and paw-biting detection in a single animal now enables the temporal relationship between mechanical pain hypersensitivity and a spontaneous pain-related behavior to be assessed.

These results indicate that an extended unilateral decrease in paw luminance during spontaneous behaviors over many minutes can be readily quantified as an averaged ratio and

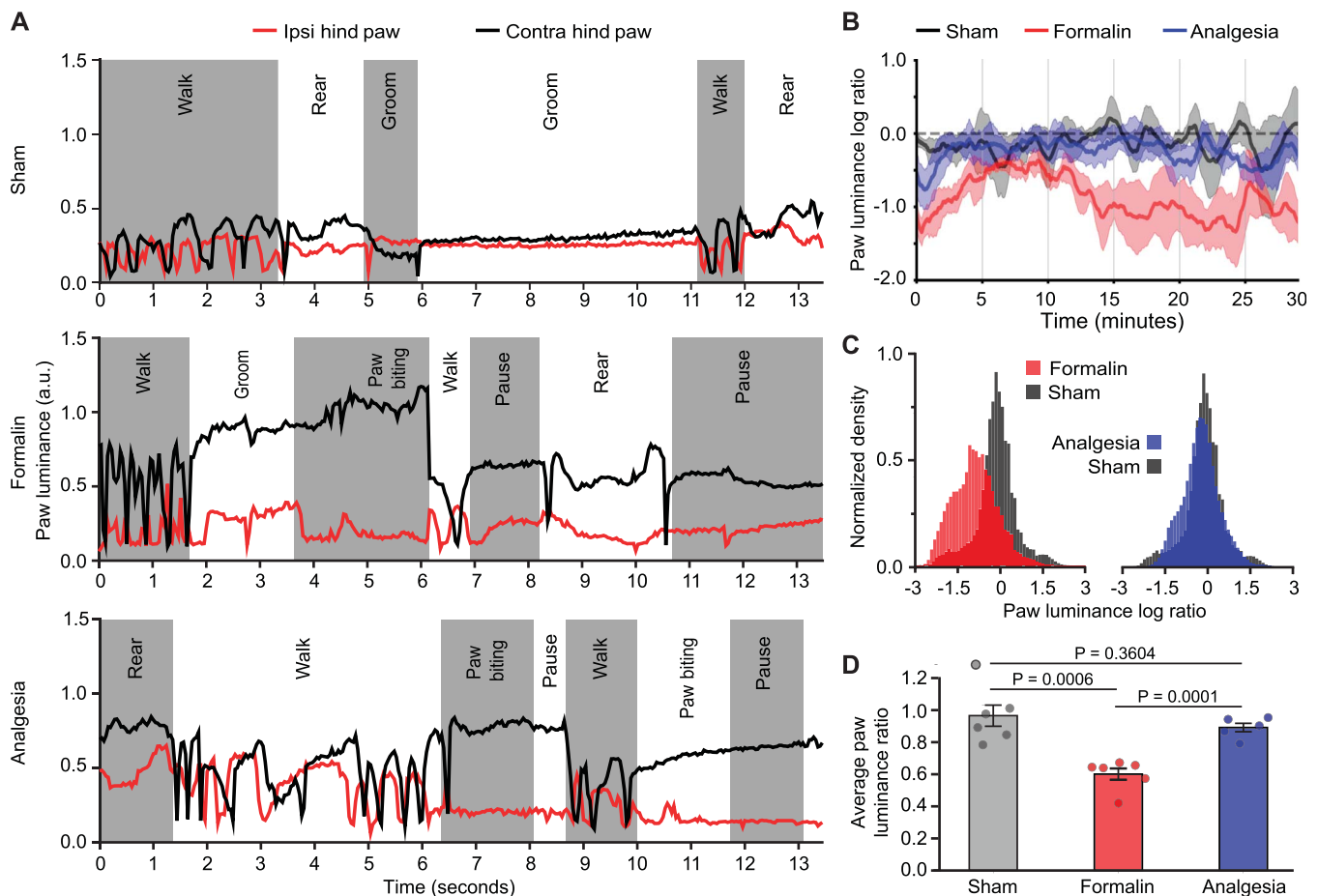


Figure 2. FTIR paw luminance signals capture pain-related and analgesia-related changes in the intraplantar formalin model. (A) Example of scaled (min-95 quantile) paw luminance signals of ipsilateral (red) and contralateral hind paw (black) of mice from sham (intraplantar saline) (top), formalin (middle), and morphine analgesia groups (3 mg/kg subcutaneous injection, bottom) during different behaviors. (B) Logarithm of paw luminance ratio (calculated as logarithmic $\left(\frac{\text{luminance}_{\text{ipsilateral-paw}}}{\text{luminance}_{\text{contralateral-paw}}}\right)$, log ratio) over the 30 minutes after intraplantar formalin/saline injection ($n = 6, 6,$ and 5 for sham, formalin, and analgesia groups). (C) Density histograms of paw luminance log ratio over a 30-minute recording of mice from sham (black, $n = 6$), formalin (red, $n = 6$), and analgesia groups (blue, $n = 5$). Formalin reduced the log ratio, and this was returned to control levels by morphine. (D) Average paw luminance ratio over a 30-min recording of mice in the 3 groups ($n = 6, 6,$ and 5) detected both the mechanical pain hypersensitivity induced by formalin and the analgesic efficacy of morphine. Shading in panel (B) indicates 95% confidence interval as mean $\pm 1.96 \times \text{SEM}$. Data in panel (D) presented as mean $\pm \text{SEM}$. Statistical significance for panel D determined by the 2-tail unpaired Student t test. FTIR, frustrated total internal reflection.

serves as a robust indicator of ongoing mechanical pain in a unilateral hind limb. The decreased average paw luminance ratio is a composite of mechanical pain-induced changes across a range of naturalistic behaviors, including gait alteration during walking; weight redistribution between hind paws while grooming, pausing, and rearing; as well as an increased frequency of ipsilateral pain-elicited behaviors such as paw biting and paw guarding. The information on both the natural behavior and the mechanical sensitivity of freely behaving animals simultaneously captured by the recording device enables us not only to extract multiple behavioral features indicating mechanical pain and analgesia, without applying a stimulus, but also to identify unwanted side effects of drugs, such as sedation or hyperlocomotion. Unsupervised learning-based methods therefore have promise for detecting novel pain-related and analgesia-related behavioral features in freely moving animals in an unbiased manner.^{12,35}

3.3. Paw luminance phenotypes multiple pain states

Robust decreases in the average paw luminance ratio were also observed in a set of unilateral hind limb pain models that capture

multiple unique and different pain states, including inflammatory models associated with a burn injury (plantar ultraviolet radiation burn model, UVB, $n = 6$, 48 hours after injury), local pathogen invasion/infection (intraplantar zymosan injection model²¹ (zymosan is a glucan ligand found on the surface of fungi), zymosan, $n = 5$, 4 hours after injury), and traumatic injury (paw skin incision model, $n = 8$, 1 hour after injury), as well as neuropathic pain (spared nerve injury model,⁹ SNI, $n = 8$, recorded at 8 weeks after injury), and knee joint inflammation (knee CFA injection model,¹⁷ $n = 6$, 3 days after injury) (Fig. 3A).

Paw luminance signals from individual recordings from mice subjected to the knee CFA injection and the SNI models demonstrated that both models induced profound surface contact force asymmetry between the 2 hind limbs, as compared to untreated control animals (Fig. 3B and C). Further investigation is needed to determine whether the decrease in the average paw luminance ratio in the SNI model is caused by underlying mechanical pain hypersensitivity alone, or motor dysfunction due to muscle denervation, or a combination of both.

To explore whether paw luminance measurements capture functional recovery after peripheral nerve injury, we used a sciatic nerve crush injury model ($n = 5$) that has been used extensively to

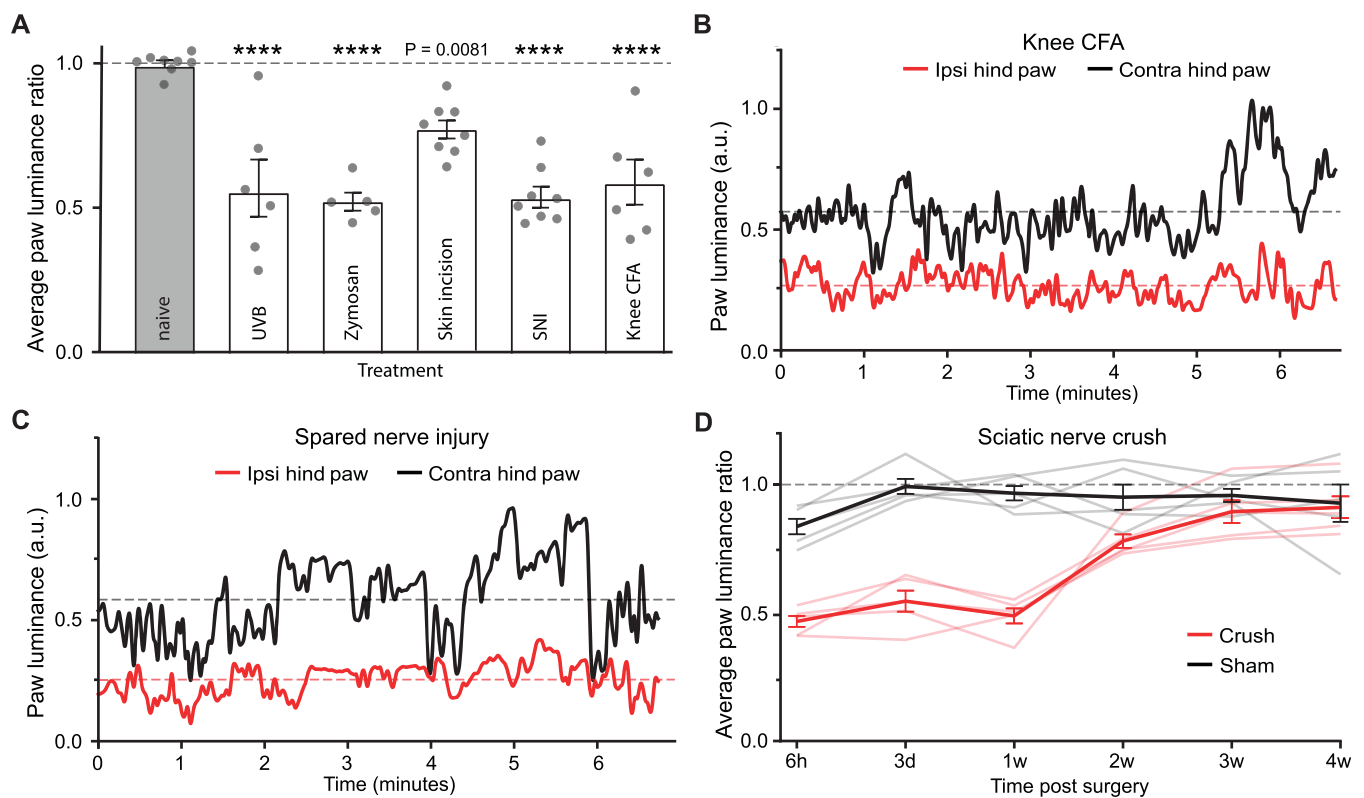


Figure 3. Paw luminance measurements in multiple unilateral pain models. (A) Average paw luminance ratios over 10 minutes for untreated mice (naive, $n = 8$), after ultraviolet radiation burn (48 hours after injury, $n = 6$), local pathogen-induced inflammation (zymosan, 4 hours after injury, $n = 5$), traumatic injury (skin incision, 1 hour after injury, $n = 8$), neuropathic pain (SNI, $n = 8$, 8 weeks after injury), and joint inflammation (knee CFA, $n = 6$, 3 days after injury). (**** $P < 0.0001$). (B) Example of scaled (min-95 quantile) paw luminance signals of both ipsilateral (red) and contralateral hind paws (black) of a mouse with knee CFA-induced inflammation. (C) Example of scaled (min-95 quantile) paw luminance signals of a mouse from the SNI model at 8 weeks after surgery. (D) Average paw luminance ratio over 20-minute recording captures functional recovery in 4 weeks after SNI (crush, red, $n = 5$), compared with the sham group (black, $n = 5$). The measures of individual mice are shown as shaded lines. Data in panel A and D presented as mean \pm SEM. Statistical significance for panel A determined by the Dunnett multiple comparison test and in D by the 2-tail unpaired Student t test. CFA, complete Freund adjuvant; SNI, sciatic nerve crush; SNI, spared nerve injury; UVB, ultraviolet radiation burn.

study peripheral nerve injury repair with a range of motor and sensory assessments.^{5,34} The average paw luminance ratios over 20 minutes indicated that sciatic nerve crush-injured mice exhibited functional recovery of paw contact as early as 2 weeks after injury (Fig. 3D), in contrast with the persistent changes observed in the SNI model (Supplemental Fig. S3, available at <http://links.lww.com/PAIN/B641>). Together, these findings indicate that this method can be used as a sensitive behavioral readout for functional recovery after nerve injury.

3.4. Quantifying in vivo analgesic actions

To probe the utility of our method in quantifying the in vivo efficacy of analgesics, we measured the average paw luminance ratio over 10 minutes in 2 inflammatory pain models, the UVB model and the zymosan model. We then compared the performance of the paw luminance assay against changes in mechanical withdrawal threshold hypersensitivity measured by the von Frey assay in response to treatment with the nonsteroidal anti-inflammatory drug ketorolac. Decreases in average paw luminance ratios of inflamed to uninjured hind paws (Fig. 3A) matched the mechanical withdrawal threshold hypersensitivity presented in the von Frey assay (Supplemental Fig. S4A, available at <http://links.lww.com/PAIN/B641>). Both the mechanical hypersensitivity induced in the UVB model and the analgesic effect of ketorolac were readily revealed by paw luminance measurements from individual animals (Fig. 4A), an indication of the low interanimal

variation of this measurement, which shows that it could be used to accurately assess mechanical pain in small numbers of animals. The decrease in average paw luminance ratios in the UVB model was reversed by systemic administration of ketorolac at 10 mg/kg (Fig. 4B, $n = 5$ for each group).

We then compared paw luminance and von Frey threshold changes in intraplantar zymosan-administered mice when treated with 3 different doses of ketorolac (1, 3, or 10 mg/kg; $n = 5$ for each group). Although the effect of ketorolac, even at the highest dose tested on von Frey mechanical hypersensitivity in this inflammatory model, was not significant compared with the saline control (Fig. 4C), the average paw luminance ratio showed a significant reversal after both 3 and 10 mg/kg ketorolac treatment with P values of 0.0334 and 0.0445, respectively (Fig. 4D). A significant effect of the high-dose ketorolac (10 mg/kg) was captured with von Frey mechanical hypersensitivity measures with a P value of 0.011, but only with a group size of 10 (Supplemental Fig. S4B, available at <http://links.lww.com/PAIN/B641>), whereas a high significance was detectable with the paw luminance ratio with a group size of 5 (Fig. 4D). We conclude, therefore, that the paw luminance measurement of mechanical pain is more sensitive than the von Frey assay in detecting the analgesic effect of ketorolac on mechanical pain in this model and that the 2 measures capture different features, an evoked response to an applied static punctate mechanical stimulus (von Frey) and a shift in paw surface contact from the injured to the control paw over an extended period during freely moving

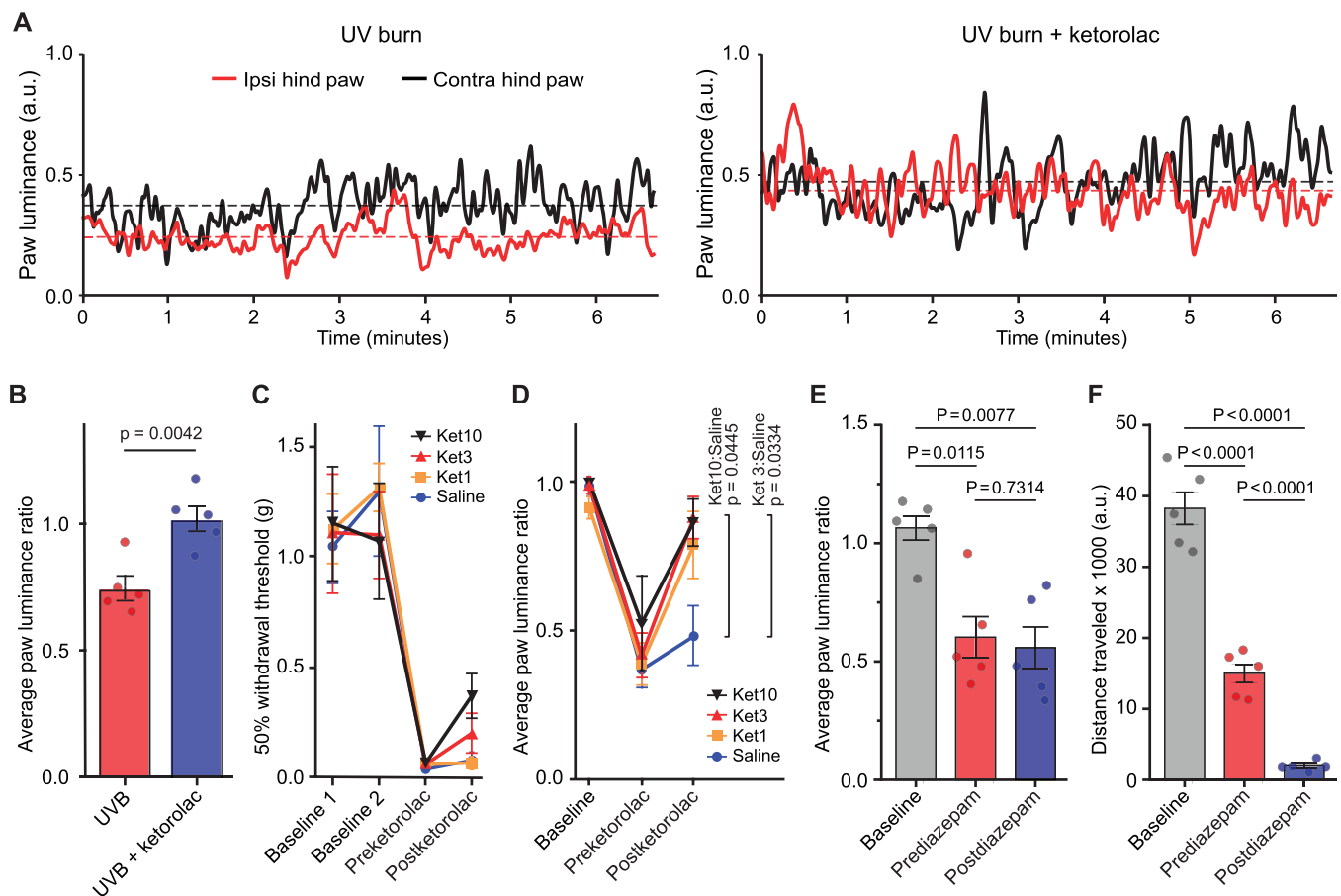


Figure 4. Average paw luminance ratio evaluation of analgesia in the inflammatory pain model. (A) Paw luminance signals of an individual animal show mechanical hypersensitivity in the injured paw (left hind paw) induced by UVB (left panel) detected by reduced luminance and increased luminance as a measure of the analgesic effect of ketorolac (10 mg/kg, right panel). (B) Ketorolac 10 mg/kg recovered the average paw luminance ratio in UVB mice to control (ratio = 1) levels ($n = 5$ for each group). (C) Effect of ketorolac (1 mg/kg, 3 mg/kg, 10 mg/kg, and saline control; $n = 5$ for each group) on von Frey mechanical thresholds and (D) on the average paw luminance ratio. Baseline readouts were conducted before zymosan injection, the “pre” readouts were 4 hours after zymosan injection but before ketorolac administration, and the “post” were 1 hour after ketorolac administration. For the average paw luminance ratio, a significant reversal from saline levels was detected after 3 and 10 mg/kg ketorolac treatment. (E) Average paw luminance ratio and (F) total distance traveled (in pixel unit) and for 10-minute recordings, baseline readouts were conducted before zymosan injection, the “pre” readouts were 4 hours after zymosan injection but before diazepam administration, and the “post” were 30 minutes after diazepam. Data in panel (B), (C), (D), (E), and (F) presented as mean \pm SEM. Statistical significance for panel (B) determined by the 2-tail unpaired Student *t*-test; for (C) and (D) by 2-way ANOVA repeated measures, followed by the Dunnett post hoc analysis; and for (E) and (F) by the paired Student *t*-test. UVB, ultraviolet radiation burn.

behavior. Based on the body surface area and the Food and Drug Administration guidance,⁸ 3 to 10 mg/kg is approximately equivalent to the human dose used in the clinical settings (0.25–1 mg/kg), indicating that the paw luminance measurement can pick up analgesic effects in mice at clinically relevant human doses.

Furthermore, the paw luminance measurement distinguishes analgesic effects from sedative activity. Diazepam induces significant sedation in mice at 2 mg/kg dosage²³ without any reported analgesic effect. We extracted both the distance traveled and the average paw luminance ratio in mice ($n = 5$) recorded for 10 minutes at baseline and 4 hours after intraplantar zymosan injection. The zymosan injection resulted in a reduction in the average paw luminance ratio (Fig. 4E) and a decrease in locomotion (Fig. 4F), both of which represent consequences of the pain the animal experiences. Diazepam (5 mg/kg, $n = 5$) was then administered to the zymosan-treated mice and 10-minute recordings made 30 minutes later. Diazepam-induced sedation was captured by a significant further decrease in locomotion (Fig. 4F), but the decreased average paw luminance ratio produced by the zymosan was not changed by the diazepam administration

(Fig. 4E), indicating that the asymmetry in paw luminance in mice with inflammatory pain continued to be detectable even when mice were sedated and that a reduction in locomotion could be caused both by pain and sedation. By contrast, morphine increased locomotion and yet normalized the average paw luminance ratio in the formalin model.

4. Discussion

Incorporating integrated body pose and FTIR data acquisition with machine learning in multiple unilateral animal pain models shows we can readily capture behavioral features indicating the presence of ongoing mechanical pain. Dynamic paw luminance represents an objective and highly sensitive indicator of mechanical pain and/or motor dysfunction in multiple different inflammatory or neuropathic disease states. From the FTIR measurements of mechanical pain hypersensitivity, we constructed a readily scalable assay for *in vivo* analgesic efficacy determination and benchmarked its superior performance in detecting analgesic effects against the conventional von Frey mechanical pain hypersensitivity assay. We also show that the

platform can also be used to screen for drug side effects, such as hyperlocomotion or sedation. We have identified, therefore, a way of measuring dynamic changes in mechanical pain hypersensitivity over time in an unbiased, observer-independent manner, without the need for any applied stimulation, that is a highly sensitive indicator of the presence of this form of pain and its disruption by analgesics. We list the multiple differences between the von Frey and the paw luminance assays in Table S1 (available at <http://links.lww.com/PAIN/B641>). The von Frey assay is suitable for specific requirements, such as quantifying static mechanical thresholds of defined areas, whereas our approach detects mechanical pain in limbs over time.

The bottom-up imaging technology is also very different from existing locomotion analysis platforms (eg, CatWalk and DigiGait), which have been used to measure pain and analgesia in rodents.^{4,33} First, our measure is based on spontaneous behavior over tens of minutes, whereas the others are based on either involuntary walking on a treadmill or walking across a narrow corridor over seconds in the light and in the presence of an observer. Second, those platforms require training sessions for animals to learn the walking task and manual correction of mislabeled frames in data processing, whereas our method requires no animal training or human supervision.

The data processing for the paw luminance assay is automated and requires minimal human input time, which could be expanded to parallel processing of multiple recordings with sufficient computing resources. The computation time for processing a single 30-minute recording on a consumer-grade PC (hardware specifications in Methods) was about 2.5 hours. More specifically, the preprocessing step for generating video files from the raw data took ~2 hours, the DeepLabCut processing time was ~15 minutes, automated behavior classification took ~25 seconds, and extracting paw luminance signal took ~2.5 minutes.

By providing a continuous recording of a freely moving mouse in the dark from below, together with a synchronized high-fidelity body surface contact measurement, and with automatic feature extraction pipelines, we believe that this technology will have utility for characterizing a broad range of physiological and pathological phenomena beyond ipsilateral hind limb pain models, such as visceral or chronic spontaneous neuropathic pain, and in detecting and quantifying the behavioral consequences of many conditions such as sedation, malaise, anxiety, and neurodegenerative and other neurological diseases.

Conflict of interest statement

D. P. Roberson, C. J. Woolf, A. B. Wiltschko, L. B. Barrett, and S. R. Datta have issued patents on the data acquisition technology. D. P. Roberson, L. B. Barrett, and C. J. Woolf have a financial relationship with Blackbox Bio, the company which has licensed the patent on the technology from Boston Children's Hospital. D. P. Roberson is also now an employee of Blackbox Bio.

Acknowledgements

This project was funded by grants from the Defense Advanced Research Projects Agency (HR0011-19-2-0022, C. J. Woolf), NIH NINDS (F31 NS084716-02, D. P. Roberson; R35 NS105076, C. J. Woolf; R01 NS089521, C. D. Harvey; F31 NS108450, J. P. Bohoslav; and R01 NA114202, S. R. Datta), the Bertarelli Foundation (C. J. Woolf), the Simons Collaboration on the Global Brain (S. R. Datta), the NIH BRAIN Initiative (U19 NS113201, S. R. Datta; U24 NS109520, S. R. Datta; and R01AT011447,

C. J. Woolf), and financial contributions from the Boston Children's Hospital Technology Development Fund. This paper does not reflect the position or the policy of the Government, and no official endorsement should be inferred. N. L. M. Quintão and V. Fattori thank the National Council for Scientific and Technological Development (CNPq, Brazil) for the postdoctoral fellowship (PDE, CNPq, process # 229356/2013-3) and Split Fellowship (Doutorado Sanduiche SWE, CNPq), respectively. The authors thank Alexander Mathis and Mackenzie Mathis for their help in implementing DeepLabCut and Michael Do for helpful suggestions for optimizing data capture. The authors thank Johannes Bill and Jan Drugowitsch for helpful discussions on data analysis and modeling.

Author contributions: D. P. Roberson and Z. Zhang contributed equally. D. P. Roberson conceived and built the data acquisition system with assistance from L. B. Barrett and wrote the control software for paired video acquisition. Z. Zhang coordinated and integrated the overall data analysis. D. P. Roberson, C. J. Woolf, B. Boivin, N. K. Wimalasena, and Z. Zhang wrote the manuscript. D. P. Roberson, B. Boivin, Z. Zhang, V. Fattori, N. K. Wimalasena, D. A. Yarmolinsky, D. G. Taub, M. Kotoda, N. L. M. Quintão, and C. J. Woolf designed experiments. D. P. Roberson, B. L. Turnes, B. Boivin, Z. Zhang, N. K. Wimalasena, D. A. Yarmolinsky, D. G. Taub, M. Kotoda, R. González-Cano, N. L. M. Quintão, and N. Andrews performed behavioral experiments. R. González-Cano and B. Boivin wrote the software to measure changes in mouse activity through changes in the pixel value. B. Boivin, Z. Zhang, and D. A. Yarmolinsky implemented DeepLabCut and performed video labeling. B. Boivin, Z. Zhang, D. A. Yarmolinsky, S. Q. Neufeld, and J. P. Bohoslav wrote code for processing video data and implemented additional convolutional neural networks for classification of rodent behaviors with input from C. D. Harvey. The paw force transducer device was conceived and built by D. A. Yarmolinsky, D. G. Taub, and Z. Zhang, and A. B. Wiltschko and S. R. Datta contributed to the analysis strategy. All authors contributed to the editing of the final manuscript.

Data and code availability: Data are available from the corresponding author on reasonable request. Code used for data acquisition and analysis is available at <https://github.com/AlexZihe/palmreader>.

Appendix A. Supplemental digital content

Supplemental digital content associated with this article can be found online at <http://links.lww.com/PAIN/B641>, <http://links.lww.com/PAIN/B642>, <http://links.lww.com/PAIN/B643>, and <http://links.lww.com/PAIN/B644>.

Supplemental video content

A video abstract associated with this article can be found at <http://links.lww.com/PAIN/B661>.

Article history:

Received 24 January 2022

Received in revised form 1 April 2022

Accepted 14 April 2022

Available online 11 May 2022

References

- [1] Abbott FV, Franklin KBJ, Westbrook RF. The formalin test: scoring properties of the first and second phases of the pain response in rats. *PAIN* 1995;60:91–102.

- [2] Abdus-Saboor I, Fried NT, Lay M, Burdige J, Swanson K, Fischer R, Jones J, Dong P, Cai W, Guo X, Tao Y-X, Bethea J, Ma M, Dong X, Ding L, Luo W. Development of a mouse pain scale using sub-second behavioral mapping and statistical modeling. *Cell Rep* 2019;28:1623–34.
- [3] Berridge KC, Whishaw IQ. Cortex, striatum and cerebellum: control of serial order in a grooming sequence. *Exp Brain Res* 1992;90:275–90.
- [4] Berryman ER, Harris RL, Moalli M, Bagi CM. DigiGait™ quantitation of gait dynamics in rat rheumatoid arthritis model. *J Musculoskelet Neuronal Interact* 2009;9:89–98.
- [5] Bester H, Beggs S, Woolf CJ. Changes in tactile stimuli-induced behavior and c-Fos expression in the superficial dorsal horn and in parabrachial nuclei after sciatic nerve crush. *J Comp Neurol* 2000;428:45–61.
- [6] Bohoslav JP, Wimalasena NK, Clausing KJ, Dai YY, Yarmolinsky DA, Cruz T, Kashlan AD, Chiappe ME, Orefice LL, Woolf CJ, Harvey CD. DeepEthogram, a machine learning pipeline for supervised behavior classification from raw pixels. *eLife* 2021;10:e63377.
- [7] Bouwknecht JA, Spiga F, Staub DR, Hale MW, Shekhar A, Lowry CA. Differential effects of exposure to low-light or high-light open-field on anxiety-related behaviors: relationship to c-Fos expression in serotonergic and non-serotonergic neurons in the dorsal raphe nucleus. *Brain Res Bull* 2007;72:32–43.
- [8] Center for Drug Evaluation and Research. Guidance for industry: estimating the maximum safe starting dose in initial clinical trials for therapeutics in adult healthy volunteers. U.S. Department of Health and Human Services, Food and Drug Administration, 2005. Available at: <https://www.fda.gov/media/72309/download>
- [9] Decosterd I, Woolf CJ. Spared nerve injury: an animal model of persistent peripheral neuropathic pain. *PAIN* 2000;87:149–58.
- [10] Gonzalez-Cano R, Boivin B, Bullock D, Cornelissen L, Andrews N, Costigan M. Up-down reader: an open source program for efficiently processing 50% von Frey thresholds. *Front Pharmacol* 2018;9:433.
- [11] González-Cano R, Montilla-García Á, Ruiz-Cantero MC, Bravo-Caparrós I, Tejada MÁ, Nieto FR, Cobos EJ. The search for translational pain outcomes to refine analgesic development: where did we come from and where are we going?. *Neurosci Biobehavioral Rev* 2020;113:238–61.
- [12] Hsu AI, Yttri EA. B-SOId, an open-source unsupervised algorithm for identification and fast prediction of behaviors. *Nat Commun* 2021;12:5188.
- [13] Jones JM, Foster W, Twomey CR, Burdige J, Ahmed OM, Pereira TD, Wojcik JA, Corder G, Plotkin JB, Abdus-Saboor I. A machine-vision approach for automated pain measurement at millisecond timescales. *eLife* 2020;9:e57258.
- [14] Kim HT, Uchimoto K, Duellman T, Yang J. Automated assessment of pain in rats using a voluntarily accessed static weight-bearing test. *Physiol Behav* 2015;151:139–46.
- [15] Kingma DP, Ba J. Adam: A Method for Stochastic Optimization. *arXiv*, 2017 doi:10.48550/arXiv.1412.6980.
- [16] Langford DJ, Bailey AL, Chanda ML, Clarke SE, Drummond TE, Echols S, Glick S, Ingrao J, Klassen-Ross T, LaCroix-Fralish ML, Matsumiya L, Sorge RE, Sotocinal SG, Tabaka JM, Wong D, van den Maagdenberg AMJM, Ferrari MD, Craig KD, Mogil JS. Coding of facial expressions of pain in the laboratory mouse. *Nat Methods* 2010;7:447–9.
- [17] Latremoliere A, Latini A, Andrews N, Cronin SJ, Fujita M, Gorska K, Hovius R, Romero C, Chuaiphichai S, Painter M, Miracca G, Babaniyi O, Remor AP, Duong K, Riva P, Barrett LB, Ferreirós N, Naylor A, Penninger JM, Tegeder I, Zhong J, Blagg J, Channon KM, Johnsson K, Costigan M, Woolf CJ. Reduction of neuropathic and inflammatory pain through inhibition of the tetrahydrobiopterin pathway. *Neuron* 2015;86:1393–406.
- [18] Machado AS, Darmohray DM, Fayad J, Marques HG, Carey MR. A quantitative framework for whole-body coordination reveals specific deficits in freely walking ataxic mice. *eLife* 2015;4:e07892.
- [19] Mathis A, Mamidanna P, Cury KM, Abe T, Murthy VN, Mathis MW, Bethge M. DeepLabCut: markerless pose estimation of user-defined body parts with deep learning. *Nat Neurosci* 2018;21:1281–9.
- [20] McNamara CR, Mandel-Brehm J, Bautista DM, Siemens J, Deranian KL, Zhao M, Hayward NJ, Chong JA, Julius D, Moran MM, Fanger CM. TRPA1 mediates formalin-induced pain. *Proc Natl Acad Sci U S A* 2007;104:13525–30.
- [21] Meller ST, Gebhart GF. Intraplantar zymosan as a reliable, quantifiable model of thermal and mechanical hyperalgesia in the rat. *Eur J Pain* (London, England) 1997;1:43–52.
- [22] Murphy NP, Lam HA, Maidment NT. A comparison of morphine-induced locomotor activity and mesolimbic dopamine release in C57BL/6, 129Sv and DBA2 mice. *J Neurochem* 2001;79:626–35.
- [23] Pádua-Reis M, Nôga DA, Tort ABL, Blunder M. Diazepam causes sedative rather than anxiolytic effects in C57BL/6J mice. *Sci Rep* 2021;11:9335.
- [24] Reynolds S, Urruela M, Devine DP. Effects of environmental enrichment on repetitive behaviors in the BTBR T+tf/J mouse model of autism. *Autism Res* 2013;6:337–43.
- [25] Roberson David P. Analysis of Voluntary Behavior to Interrogate Neural Function, 2016. Doctoral dissertation, Harvard University, Graduate School of Arts & Sciences. Available at: <http://nrs.harvard.edu/urn-3.HUL.InstRepos:26718761>.
- [26] Sadler KE, Mogil JS, Stucky CL. Innovations and advances in modelling and measuring pain in animals. *Nat Rev Neurosci* 2022;23:70–85.
- [27] Shimada SG, LaMotte RH. Behavioral differentiation between itch and pain in mouse. *PAIN* 2008;139:681–7.
- [28] Sorge RE, Martin LJ, Isbester KA, Sotocinal SG, Rosen S, Tuttle AH, Wieskopf JS, Acland EL, Dokova A, Kadoura B, Leger P, Mapplebeck JCS, McPhail M, Delaney A, Wigerblad G, Schumann AP, Quinn T, Frasnelli J, Svensson CI, Sternberg WF, Mogil JS. Olfactory exposure to males, including men, causes stress and related analgesia in rodents. *Nat Methods* 2014;11:629–32.
- [29] Sotocina SG, Sorge RE, Zaloum A, Tuttle AH, Martin LJ, Wieskopf JS, Mapplebeck JC, Wei P, Zhan S, Zhang S, McDougall JJ, King OD, Mogil JS. The rat grimace scale: a partially automated method for quantifying pain in the laboratory rat via facial expressions. *Mol Pain* 2011;7:55.
- [30] Sufka KJ. Conditioned place preference paradigm: a novel approach for analgesic drug assessment against chronic pain. *PAIN* 1994;58:355–66.
- [31] Tétreault P, Dansereau M-A, Doré-Savard L, Beaudet N, Sarret P. Weight bearing evaluation in inflammatory, neuropathic and cancer chronic pain in freely moving rats. *Physiol Behav* 2011;104:495–502.
- [32] Voisin T, Perner C, Messou M-A, Shiers S, Ualiyeva S, Kanaoka Y, Price TJ, Sokol CL, Bankova LG, Austen KF, Chiu IM. The CysLT2R receptor mediates leukotriene C4-driven acute and chronic itch. *Proc Natl Acad Sci U S A* 2021;118:e2022087118.
- [33] Vrinten DH, Hamers FFT. ‘CatWalk’ automated quantitative gait analysis as a novel method to assess mechanical allodynia in the rat; a comparison with von Frey testing. *PAIN* 2003;102:203–9.
- [34] Wang T, Ito A, Aoyama T, Nakahara R, Nakahata A, Ji X, Zhang J, Kawai H, Kuroki H. Functional evaluation outcomes correlate with histomorphometric changes in the rat sciatic nerve crush injury model: a comparison between sciatic functional index and kinematic analysis. *PLoS One* 2018;13:e0208985.
- [35] Wiltschko AB, Johnson MJ, Iurilli G, Peterson RE, Katon JM, Pashkovski SL, Abraira VE, Adams RP, Datta SR. Mapping sub-second structure in mouse behavior. *Neuron* 2015;88:1121–35.
- [36] Xu Y, Tian N-X, Bai Q-Y, Chen Q, Sun X-H, Wang Y. Gait assessment of pain and analgesics: comparison of the DigiGait™ and CatWalk™ gait imaging systems. *Neurosci Bull* 2019;35:401–18.
- [37] Zhang H, Lecker I, Collymore C, Dokova A, Pham MC, Rosen SF, Crawhall-Duk H, Zain M, Valencia M, Filippini HF, Li J, D’Souza AJ, Cho C, Michailidis V, Whissell PD, Patel I, Steenland HW, Virginia Lee W-J, Moayedil M, Sterley T-L, Bains JS, Stratton JA, Matyas JR, Biernaskie J, Dubins D, Vukobradovic I, Bezginov A, Flenniken AM, Martin LJ, Mogil JS, Bonin RP. Cage-lid hanging behavior as a translationally relevant measure of pain in mice. *PAIN* 2021;162:1416–25.